CHIN. PHYS. LETT. Vol. 35, No. 8 (2018) 087501

# Tunneling Anisotropic Magnetoresistance in $L1_0$-MnGa Based Antiferromagnetic Perpendicular Tunnel Junction *

Xu-Peng Zhao(赵旭鹏)[1,2], Da-Hai Wei(魏大海)[1,2], Jun Lu(鲁军)[1,2], Si-Wei Mao(毛思玮)[1,2], Zhi-Feng Yu(余之峰)[1,2], Jian-Hua Zhao(赵建华)[1,2]**

[1]*State Key Laboratory of Superlattices and Microstructures, Institute of Semiconductors, Chinese Academy of Sciences, Beijing 100083*

[2]*College of Materials Science and Opto-Electronic Technology, University of Chinese Academy of Sciences, Beijing 100049*

(Received 11 April 2018)

*We report on the tunneling anisotropic magnetoresistance in antiferromagnetic perpendicular tunnel junction consisting of $L1_0$-MnGa/FeMn/$AlO_x$/Pt grown on GaAs (001) substrates by molecular-beam epitaxy. The temperature-dependent perpendicular exchange bias effect reveals an exchange coupling between ferromagnetic $L1_0$-MnGa and antiferromagnetic FeMn. The rotation of antiferromagnetic spins in FeMn can be driven by perpendicularly magnetized $L1_0$-MnGa due to the exchange-spring effect at the interface and leads to room-temperature tunneling anisotropic magnetoresistance ratio of 0.86%. We also find that the tunneling anisotropic magnetoresistance strongly depends on temperature and angle. These results have broadened the material selection range for high performance antiferromagnetic spintronic devices.*

*PACS:* 75.50.Ee, 75.30.Et, 75.50.Vv, 75.47.−m, 81.15.Hi DOI: 10.1088/0256-307X/35/8/087501

Antiferromagnetic (AFM) spintronics is an emerging field and has drawn wide interest in recent years due to its innate characters, such as high stability to a parasitic magnetic field, no stray field, and high-frequency dynamics.[1,2] Generally, the ferromagnetic (FM) materials are working as key elements in generating spin-polarized charge currents or pure spin currents in various conventional spintronic phenomena,[3] while the AFM materials usually play a passive role and are used to introduce exchange bias on adjacent FM layers. In AFM spintronic devices, the spin-dependent transport properties are designed to be governed by AFM materials, which have shown unique advantages. Distinct from a conventional tunnel magnetoresistance (TMR) effect with two FM electrodes, the tunnel anisotropic magnetoresistance (TAMR) effect was first observed in ferromagnet-based structure with only one magnetic electrode, such as (Ga,Mn)As/GaAs, Fe/GaAs/Au and [Co/Pt]/$AlO_x$/Pt junctions,[4−7] which is associated with the anisotropic density of states (DOS) and does not rely on the spin-coherent quantum interference. However, it has been proposed that this phenomenon should be equally present in AFM materials. Notably, the TAMR effect has opened a new route for AFM spintronics. Hence, much work has been focused on the TAMR effect in the AFM tunnel junction.

It is worth mentioning that beyond the current passive role of AFM in pinning FM, spins in ultrathin AFM could also be motivated by the neighboring FM, leading to the exchange-spring effect at the interface.[8] Therefore, the rotation of AFM spins is staggered by adjacent FM layers with the exchange-spring effect, which influences the tunneling DOS and further brings about a TAMR signal in the AFM tunnel junction. The utilization of the exchange-spring effect is of great demand because it is crucial for manipulating AFM spins as well as realizing the functionality of the AFM layer. Moreover, the TAMR also provides a new method to investigate the transport behavior of antiferromagnetically ordered moments in the AFM layer coupled with the FM layer.[8−10] In 2011, Park *et al.* first demonstrated the in-plane TAMR in the AFM tunnel junction governed by the IrMn coupled with in-plane magnetized NiFe.[11] In 2015, Wang *et al.* observed in-plane TAMR in an AFM tunnel junction with AFM insulator CoO.[12] Unfortunately, the TAMR measurements mentioned above were performed at low temperature and disappeared above 100 K, which limits their further practical applications. On the other hand, the materials with perpendicular magnetic anisotropy (PMA) are of great significance since they have a potential of realizing nonvolatile magnetic random-access memory (MRAM).[13−15] Hence, room-temperature (RT) out-of-plane TAMR is more desirable for future applications of AFM spintronic devices. In 2012, Wang

*Supported by the National Basic Research Program of China under Grant No 2015CB921500, the National Natural Science Foundation of China under Grant Nos 61334006 and 11774339, the Key Research Project of Frontier Science of the Chinese Academy of Sciences under Grant No QYZDY-SSW-JSC015, and the Key Research Program of the Chinese Academy of Sciences under Grant No XDPB08-2.

**Corresponding author. Email: jhzhao@red.semi.ac.cn

© 2018 Chinese Physical Society and IOP Publishing Ltd

*et al.* first demonstrated RT out-of-plane TAMR in $[Co/Pt]_n/IrMn/AlO_x/Pt$ tunnel junctions, which was attributed to the superior thermal tolerance of perpendicular exchange coupling and stable AFM spins in IrMn.[16,17] However, the RT out-of-plane TAMR ratio in the AFM tunnel junction is still relatively low and needs further improvements.

It is believed that the out-of-plane TAMR strongly depends on the perpendicular exchange coupling behavior in the specific FM/AFM system. Among the various PMA materials, $L1_0$-MnGa alloy has exhibited many attractive properties, such as large PMA, small Gilbert damping constant and high spin polarization, making it an excellent candidate material for novel spintronic devices.[18–20] In addition, FeMn is a typical noncoplanar antiferromagnet with high Neel temperature ($T_N \sim 500$ K) and 3Q spin structure. Compared with NiMn and PtMn, FeMn is in AFM phase in the as-deposited state and does not require a high temperature anneal and large thickness.[21–23] Recently, we have demonstrated a large spontaneous perpendicular exchange bias effect in $L1_0$-MnGa/FeMn bilayers.[24] Compared with the $[Co/Pt]_n$ multilayer used in previous perpendicular AFM tunnel junctions, $L1_0$-MnGa shows a higher coercive force and better thermal stability. The strong perpendicular exchange coupling between $L1_0$-MnGa and FeMn gives rise to an enhanced exchange-spring effect, which can drive the rotation of AFM spins.

In this Letter, we explore a new FM/AFM system composed of FM $L1_0$-MnGa with strong PMA and AFM FeMn. We have investigated the out-of-plane TAMR effect in the AFM tunnel junction consisting of the $L1_0$-MnGa/FeMn/$AlO_x$/Pt stacking structure. Both the temperature and angle dependence of the TAMR signal are investigated in detail to obtain a deep insight into the transport behavior of AFM spins of FeMn.

The multilayer of $L1_0$-MnGa (12 nm)/FeMn (4 nm)/$AlO_x$ (2 nm)/Pt (10 nm) was grown on GaAs (001) substrates by molecular-beam epitaxy (MBE). Two MBE growth chambers (left and right), which were interconnected by an ultra-high-vacuum preparation chamber, were used to grow a GaAs buffer layer and $L1_0$-MnGa/FeMn/$AlO_x$/Pt multilayers, respectively. After growth of the $L1_0$-MnGa layers on GaAs (001) surfaces at 250°, the substrates were cooled down to room temperature for the deposition of FeMn layers. The nominal atomic composition ratio of Fe:Mn is set at 50:50. The crystalline structure of the multilayer was investigated by x-ray diffraction (XRD). The magnetic measurements have been carried out using the quantum design superconducting quantum interference device (SQUID) magnetometry. The magnetic multilayer was then patterned into rectangle-shaped pillars of $40 \times 40\,\mu m^2$ using photolithography combined with the ion milling technique. The TAMR was measured by four-point contact geometry in a Quantum Design physical property measurement system (PPMS). The measurements of magnetic properties and electric transport behaviors were performed without any field cooling procedures. The data were recorded with the magnetic field changing from $+H_{max}$ to $-H_{max}$ and then returning back to $+H_{max}$.

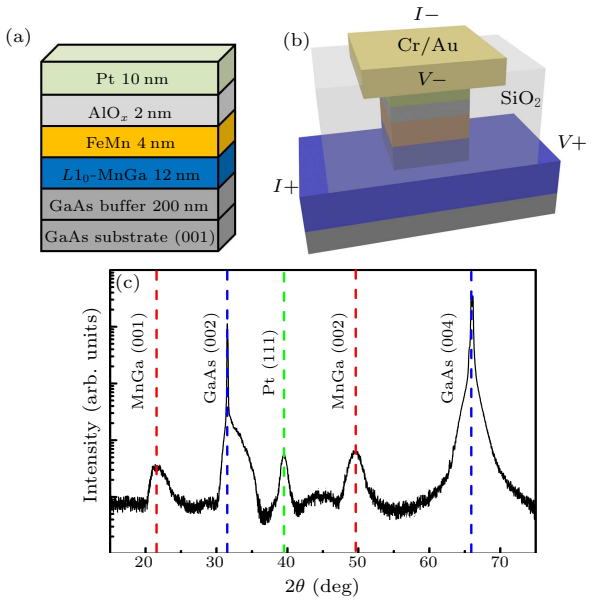


**Fig. 1.** (a) The layer stacking structure of the sample. (b) Three-dimensional schematic of $L1_0$-MnGa/FeMn/$AlO_x$/Pt tunnel junction. (c) The XRD pattern of the $L1_0$-MnGa/FeMn/$AlO_x$/Pt multilayer.

As shown in Fig. 1(a), the multilayer consisting of $L1_0$-MnGa (12 nm)/FeMn (4 nm)/$AlO_x$ (2 nm)/Pt (10 nm) was epitaxially grown on the GaAs (001) substrate with the epitaxial relationship of MnGa(001)[100]//GaAs(001)[110].[18] A 10-nm-thick Pt layer was deposited on the $AlO_x$ barrier layer, which works as normal metal and protects the multilayer from oxidation. Figure 1(b) shows the three-dimensional schematic of the tunnel junction device. The magnetoresistance of the patterned $L1_0$-MnGa/FeMn/$AlO_x$/Pt tunnel junction was measured in a four-terminal geometry with a bias current of 200 μA. Figure 1(c) shows the XRD $\theta$–$2\theta$ pattern of the as-grown $L1_0$-MnGa/FeMn/$AlO_x$/Pt multilayer. The superlattice (001) and fundamental (002) peaks of $L1_0$-MnGa films can be observed at $2\theta = 21.9°$ and 49.6°, respectively, which indicates the excellent crystal quality of the $L1_0$-MnGa. The lattice constant of face-centeredcubic FeMn is 3.63 Å, which is nearly the same as the out-of-plane lattice constant $c$ of $L1_0$-MnGa (3.64 Å). Therefore, the diffraction peaks of polycrystalline FeMn are relatively weak and mixed with that of $L1_0$-MnGa. The thin $AlO_x$ layer formed by oxidizing the 2-nm-thick aluminum in dry

air tends to be polycrystalline and its diffraction peaks are relatively weak. Furthermore, the peak observed at $2\theta = 39.7°$ corresponds to the (111) peak of Pt top electrodes.

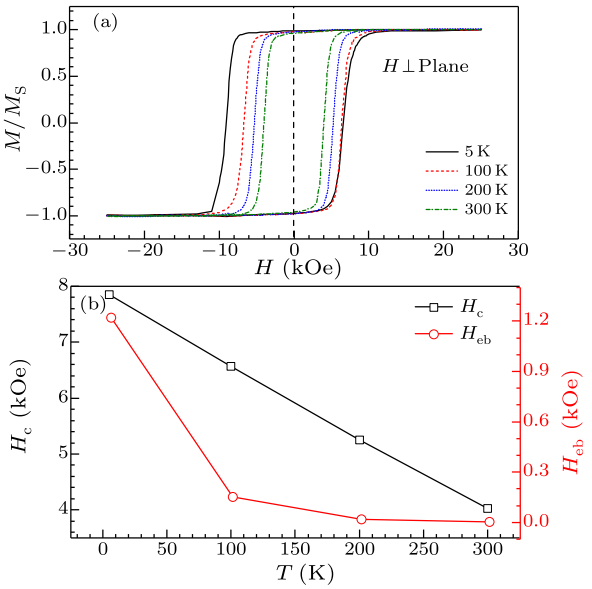


**Fig. 2.** (a) The out-of-plane hysteresis loops of $L1_0$-MnGa/FeMn/$AlO_x$/Pt multilayer. (b) The temperature dependence of perpendicular exchange bias $H_{eb}$ and coercive force $H_c$.

Figure 2(a) shows the out-of-plane hysteresis loops of $L1_0$-MnGa/FeMn/$AlO_x$/Pt multilayer measured from 5 K to 300 K. Obviously, the out-of-plane hysteresis loops are well-squared throughout all the temperature range, which indicates the strong PMA of the multilayer. As the temperature drops, the hysteresis loops show an obvious left-shift and an enhancement of coercive force $H_c$. In the exchange biased system, the exchange bias field $H_{eb}$ and coercive force $H_c$ are calculated using $H_{eb} = -(H_{c1} + H_{c2})/2$ and $H_c = |H_{c1} - H_{c2}|/2$, where $H_{c1}$ and $H_{c2}$ are the coercive forces of left and right branches, respectively. The temperature dependence of $H_{eb}$ and $H_c$ is summarized in Fig. 2(b). For the FM layer, the coercive field usually shows a typical inverse relationship with temperature because of the enhancement of the domain wall pinning effect at low temperatures.[25,26] When the Curie temperature $T_C$ of FM is higher than the Neel temperature $T_N$ of AFM, the exchange bias $H_{eb}$ usually shows a monotonically decreasing trend with increasing temperature.[27,28] In our structure, $T_C$ of bulk $L1_0$-MnGa is around 630 K, which is larger than $T_N$ of bulk FeMn (~500 K). It is noted that the thickness of the FeMn layer (4 nm) is close to the critical thickness (2–3 nm) for establishing exchange bias in the adjacent FM layer. According to Meiklejohn and Bean's model, the EB effect occurs when the condition $J_{ex} < K_{AFM} \cdot t_{AFM}$ is satisfied, where $J_{ex}$, $K_{AFM}$, and $t_{AFM}$ are the interfacial exchange coupling energy, magnetic anisotropy energy, and thickness of AFM layer, respectively.[29] Therefore, the perpendicular exchange bias $H_{eb}$ shows a maximum value of 1.2 kOe at 5 K and then gradually drops to zero because of the decrease of $K_{AFM}$.

We now focus on the temperature-dependent out-of-plane TAMR signal. Figures 3(a)–3(d) show the resistance-area (RA) product of the tunnel junction measured at 5, 100, 200, and 300 K, respectively. The inset figures show the arrangement of AFM spins of FeMn and magnetic moments in $L1_0$-MnGa. All these curves in Fig. 3 exhibit spin-valve like signals. At 5 K, the TAMR signal exhibits a clear hysteresis loop with stable high-resistance state (HRS) at $+H$ and low-resistance state (LRS) at $-H$. Generally, the traditional AMR curve of the FM film usually exhibits two symmetric small shoulders, which is significantly different from our results. Therefore, it can be concluded that the spin-valve like TAMR signals in our structure originates from the partial rotation of AFM spins of FeMn driven by $L1_0$-MnGa. Moreover, the observed asymmetry between HRS and LRS can be ascribed to the downward component of interfacial AFM spins according to previous results, which is an imprint of the domain pattern of as-deposited $L1_0$-MnGa.[30,31] At $+H$, the AFM spins nearly align in the in-plane direction. Hence, the magnetization of $L1_0$-MnGa is orthogonal to the AFM spins, which leads to HRS. When it turns to $-H$, AFM spins partially rotate due to the exchange-spring effect. In this case, the parallel relationship leads to LRS of the RA curves. In addition, the RA curves do not show an obvious shift because the magnetization of bottom electrode $L1_0$-MnGa in the tunnel junction is mainly pinned by the channel.

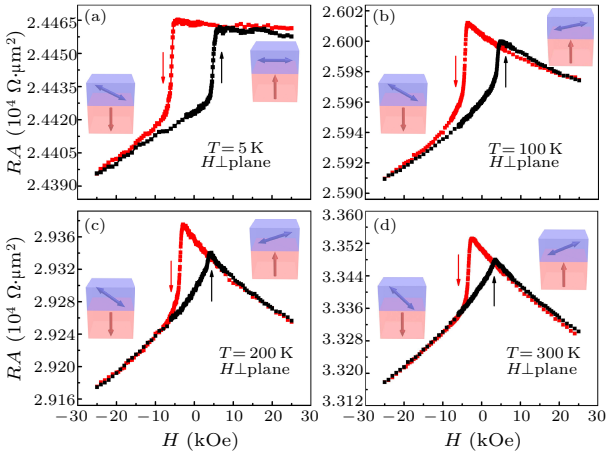


**Fig. 3.** The temperature-dependent out-of-plane TAMR measured at (a) 5 K, (b) 100 K, (c) 200 K, and (d) 300 K. The red (black) line shows the RA curve with the magnetic field swept from $+H$ ($-H$) to $-H$ ($+H$). The inset figures show the arrangement of the magnetic moment of $L1_0$-MnGa and FeMn.

To further investigate the angle dependence of the TAMR signal, the RA curves were measured at sev-

eral selected angles $\varphi$. As shown in Fig. 4(a), the RA curves measured at 5 K exhibit clear spin-valve like signals when $\varphi$ is 0°, 30°, and 60°. Considering that the TAMR effect originates from the anisotropy of tunneling DOS of AFM spins triggered by $L1_0$-MnGa, the enhancement of the transition field of RA at higher angle $\varphi$ suggests that $L1_0$-MnGa owns a larger coercive force at magnetic hard-axis direction. Furthermore, the RA nearly keeps at a high value when the magnetic field is swept at $\varphi = 90°$, which indicates that the AFM spins persistently rotate with the magnetization of $L1_0$-MnGa in the in-plane direction. As shown in Fig. 4(b), the RA curves measured at 300 K show a similar trend to that of 5 K when $\varphi < 60°$. However, the in-plane RA curve shows a different switching behavior compared with that of 5 K. Here the complex rotation behavior of AFM spins in FeMn at RT is probably originated from the competition effect between the exchange-spring effect from $L1_0$-MnGa and in-plane anisotropy of FeMn itself, which needs further systematic investigations.

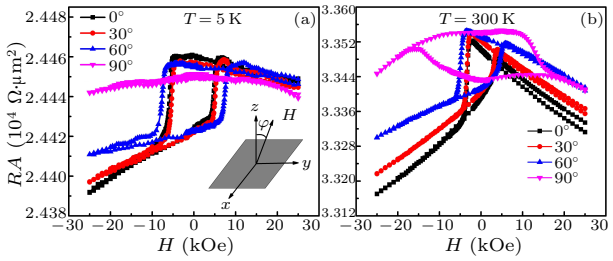


**Fig. 4.** TAMR signals measured at (a) 5 K and (b) 300 K with $\varphi$ setting at 0°, 30°, 60°, and 90°, respectively. The inset figure shows the sketches of the measurement configuration.

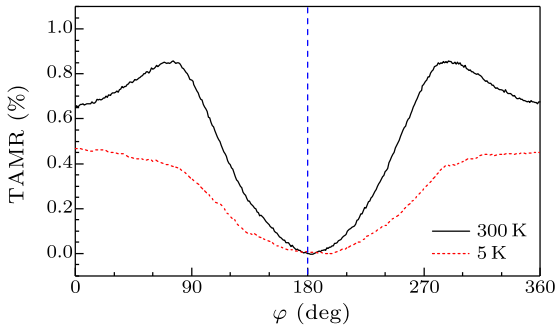


**Fig. 5.** The angular dependence of TAMR ratio measured at 5 and 300 K with $\varphi$ changing from 0° to 360° under a fixed magnetic field of 6 T.

Figure 5 shows the TAMR ratio as a function of $\varphi$ changing from 0° to 360° under a fixed magnetic field of 6 T. It is noted that the magnetization of $L1_0$-MnGa is saturated at all angles in this case. The TAMR ratio was calculated using the formula of $100\% \times (R_{\rm HRS} - R_{\rm LRS})/R_{\rm LRS}$. Specifically, $H$ was initially applied in the positive out-of-plane direction and rotated 360° to investigate the full angular dependence of the TAMR ratio. At 5 K, the TAMR ratio shows a peak value (0.45%) at 0° (360°) and reaches the minimum at 180°, which is quite in agreement with the intrinsic hysteretic nature of the AFM TAMR signals induced by the exchange-spring effect. Furthermore, the TAMR curve measured at 300 K shows a different angular dependence behavior and a larger signal of 0.86%, which is over three times larger than the previous results of 0.24% observed in the $[{\rm Co/Pt}]_n/{\rm IrMn/AlO}_x/{\rm Pt}$ tunnel junction.[16] It is noted that the anomalous angular dependence has been observed in previous results in $[{\rm Co/Pt}]_n/{\rm FeMn/AlO}_x/{\rm Pt}$.[17]

Generally, the rotation angle contributed to TAMR can be considered as the average rotation of all the AFM spins within the exchange-spring range. At low temperature, $K_{\rm AFM}$ of FeMn is large enough, which leads to a strong perpendicular exchange bias as well as a stable exchange-spring effect. Hence, the difference between HRS and LRS originated from the downward component of interfacial FeMn spins is more distinct at 5 K. As the temperature increases, $K_{\rm AFM}$ of FeMn and domain wall pinning gradually decrease, which make AFM spins easier to be motivated by the $L1_0$-MnGa at higher temperature. That is, AFM spins in FeMn tend to rotate with the magnetization of $L1_0$-MnGa, which is also shown in the inset of Fig. 3. In this case, the downward component of interfacial FeMn spins gradually decreases and the asymmetry between HRS and LRS turns to be smaller. On the other hand, the enhanced average rotation angle leads to a larger difference of tunneling DOS of AFM spins, which further results in a higher TAMR ratio observed at 300 K.

In summary, we have demonstrated the TAMR in $L1_0$-MnGa based AFM tunnel junction with the structure of $L1_0$-MnGa/FeMn/$\rm AlO_x$/Pt. The exchange coupling between $L1_0$-MnGa and FeMn is characterized by the perpendicular exchange bias. Due to the exchange-spring effect, the partial rotation of AFM spins in FeMn can be driven by perpendicularly magnetized $L1_0$-MnGa and leads to clear spin valve like TAMR signals in the tunnel junction. Specifically, the TAMR ratio reaches up to 0.86% at 300 K, which is larger than the value of 0.24% obtained by Song *et al.* in the $[{\rm Co/Pt}]_n/{\rm IrMn/AlO}_x/{\rm Pt}$ structure.[16] The angular dependence of the TAMR signal is well consistent with the hysteretic nature of the RA curves. Moreover, the asymmetry between HRS and LRS declines at higher temperature due to the reduced downward component of interfacial FeMn spins. All these results lay the foundation of the future application of AFM tunnel junction with RT out-of-plane TAMR.

## References

[1] Jungwirth T, Marti X, Wadley P and Wunderlich J 2016

*Nat. Nanotechnol.* **11** 231
[2] Baltz V, Manchon A, Tsoi M, Moriyama T, Ono T and Tserkovnyak Y 2018 *Rev. Mod. Phys.* **90** 015005
[3] Chappert C, Fert A and van Dau F N 2007 *Nat. Mater.* **6** 813
[4] Rüster C, Gould C, Jungwirth T, Sinova J, Schott G M, Giraud R, Brunner K, Schmidt G and Molenkamp L W 2005 *Phys. Rev. Lett.* **94** 027203
[5] Gould C, Rüster C, Jungwirth T, Girgis E, Schott G M, Giraud R, Brunner K, Schmidt G and Molenkamp L W 2004 *Phys. Rev. Lett.* **93** 117203
[6] Uemura T, Harada M, Matsuda K I and Yamamoto M 2010 *Appl. Phys. Lett.* **96** 252106
[7] Park B G, Wunderlich J, Williams D A, Joo S J, Jung K Y, Shin K H, Olejník K, Shick A B and Jungwirth T 2008 *Phys. Rev. Lett.* **100** 087204
[8] Scholl A, Liberati M, Arenholz E, Ohldag H and Stöhr J 2004 *Phys. Rev. Lett.* **92** 247201
[9] Martí X, Park B G, Wunderlich J, Reichlová H, Kurosaki Y, Yamada M, Yamamoto H, Nishide A, Hayakawa J, Takahashi H and Jungwirth T 2012 *Phys. Rev. Lett.* **108** 017201
[10] Ohldag H, Scholl A, Nolting F, Arenholz E, Maat S, Young A T, Carey M and Stöhr J 2003 *Phys. Rev. Lett.* **91** 017203
[11] Park B G, Wunderlich J, Martí X, Holý V, Kurosaki Y, Yamada M, Yamamoto H, Nishide A, Hayakawa J, Takahashi H, Shick A B and Jungwirth T 2011 *Nat. Mater.* **10** 347
[12] Wang K, Sanderink J G M, Bolhuis T, van der Wiel W G and de Jong M P 2015 *Sci. Rep.* **5** 15498
[13] Mangin S, Ravelosona D, Katine J A, Carey M J, Terris B D and Fullerton E E 2006 *Nat. Mater.* **5** 210
[14] Sbiaa R, Law R, Lua S Y H, Tan E L, Tahmasebi T, Wang C C and Piramanayagam S N 2011 *Appl. Phys. Lett.* **99** 092506
[15] Ikeda S, Miura K, Yamamoto H, Mizunuma K, Gan H D, Endo M, Kanai S, Hayakawa J, Matsukura F and Ohno H 2010 *Nat. Mater.* **9** 721
[16] Wang Y Y, Song C, Cui B, Wang G Y, Zeng F and Pan F 2012 *Phys. Rev. Lett.* **109** 137201
[17] Wang Y Y, Song C, Wang G Y, Zeng F and Pan F 2014 *New J. Phys.* **16** 123032
[18] Zhu L J, Nie S H, Meng K K, Pan D, Zhao J H and Zheng H Z 2012 *Adv. Mater.* **24** 4547
[19] Mizukami S, Wu F, Sakuma A, Walowski J, Watanabe D, Kubota T, Zhang X, Naganuma H, Oogane M, Ando Y and Miyazaki T 2011 *Phys. Rev. Lett.* **106** 117201
[20] Kurt H, Rode K, Venkatesan M, Stamenov P and Coey J M D 2011 *Phys. Rev.* B **83** 020405
[21] Ekholm M and Abrikosov I A 2011 *Phys. Rev.* B **84** 104423
[22] Schulthess T C, Butler W, Stocks G M, Maat S and Mankey G J 1999 *J. Appl. Phys.* **85** 4842
[23] Nakamura K, Ito T, Freeman A J, Zhong L and Fernandezdecastro J 2003 *Phys. Rev.* B **67** 014405
[24] Zhao X P, Lu J, Mao S W, Yu Z F, Wei D H and Zhao J H 2018 *Appl. Phys. Lett.* **112** 042403
[25] Paul D I 1982 *J. Appl. Phys.* **53** 1649
[26] Zhang B and Soffa W A 1994 *Scr. Metall. Mater.* **30** 683
[27] Tsang C, Heiman N and Lee K 1981 *J. Appl. Phys.* **52** 2471
[28] Ambrose T and Chien C L 1998 *J. Appl. Phys.* **83** 6822
[29] Meiklejohn W H and Bean C P 1956 *Phys. Rev.* **102** 1413
[30] Dijken S V, Crofton M, Czapkiewicz M, Zoladz M and Stobiecki T 2006 *J. Appl. Phys.* **99** 083901
[31] Brück S, Sort J, Baltz V, Suriñach S, Muñoz J S, Dieny B, Baró M D and Nogués J 2005 *Adv. Mater.* **17** 2978